Biomaterials Science

Linear and nonlinear rheology of liberase-treated breast cancer tumors

Journal:	*Biomaterials Science*
Manuscript ID	BM-ART-01-2023-000038
Article Type:	Paper
Date Submitted by the Author:	09-Jan-2023
Complete List of Authors:	Corder, Ria; North Carolina State University, Chemical and Biomolecular Engineering Vachieri, Robert; North Carolina Central University, Chemistry and Biochemistry Martin, Megan; North Carolina Central University, Biological and Biomedical Sciences Taylor, Darlene; North Carolina Central University, Chemistry and Biochemistry Fleming, Jodie; North Carolina Central University, Biological and Biomedical Sciences Khan, Saad; North Carolina State University, Chemical and Biomolecular Engineering

Linear and Nonlinear Rheology of Liberase-Treated Breast Cancer Tumors

Ria D. Corder,[1†] Robert B. Vachieri,[2] Megan E. Martin,[3] Darlene K. Taylor,[2] Jodie M. Fleming,[3‡*] and Saad A. Khan[1*]

[1]Department of Chemical and Biomolecular Engineering, North Carolina State University, Raleigh, NC, 27695, USA

[2]Department of Chemistry and Biochemistry, North Carolina Central University, Durham, NC, 27707, USA

[3]Department of Biological and Biomedical Sciences, North Carolina Central University, Durham, NC, 27707, USA

ABSTRACT

Extracellular matrix (ECM) rigidity has been shown to increase the invasive properties of breast cancer cells, promoting transformation and metastasis through mechanotransduction. Reducing ECM stiffness via enzymatic digestion could be a promising approach to slowing breast cancer development by de-differentiation of breast cancer cells to less aggressive

† Current address: Purdue University, West Lafayette, IN, 47907, USA.

‡ Current address: National Institutes of Health, Bethesda, MD, 20892, USA. *Disclaimer: This work was prepared while Jodie Fleming was employed at North Carolina Central University. The opinions expressed in this article are the author's own and do not reflect the view of the National Institutes of Health, the Department of Health and Human Services, or the United States government.*

* Co-corresponding authors (email: jodie.fleming@nih.gov, khan@eos.ncsu.edu).

phenotypes and enhancing the effectiveness of existing chemotherapeutics via improved drug penetrance throughout the tumor. In this study, we examine the effects of injectable liberase (a blend of collagenase and thermolysin enzymes) treatments on the linear and nonlinear rheology of allograft 4T1 mouse mammary tumors. We perform two sets of *in vivo* mouse studies, in which either one or multiple treatment injections occur before the tumors are harvested for rheological analysis. The treatment groups in each study consist of a buffer control, free liberase enzyme in buffer, a thermoresponsive copolymer called LiquoGel (LQG) in buffer, and a combined, localized injection of LQG and liberase. All tumor samples exhibit gel-like linear rheological behavior with the elastic modulus significantly larger than the viscous modulus and both independent of frequency. Tumors that receive a single injection of localized liberase have significantly lower tumor volumes and lower tissue moduli at both the center and edge compared to buffer- and free liberase-injected control tumors, while tissue viscoelasticity remains relatively unaffected. Tumors injected multiple times with LQG and liberase also have lower tissue volumes but possess higher tissue moduli and lower viscoelasticities compared to the other treatment groups. We propose that a mechanotransductive mechanism could cause the formation of smaller but stiffer tumors after repeated, localized liberase injections. Large amplitude oscillatory shear (LAOS) experiments are also performed on tissues from the multiple injection study and the results are analyzed using MITlaos. LAOS analysis reveals that all 4T1 tumors from the multiple injection study exhibit nonlinear rheological behavior at high strains and strain rates. Examination of the Lissajous-Bowditch curves, Chebyshev coefficient ratios, elastic moduli, and dynamic viscosities demonstrate that the onset and type of nonlinear behavior is independent of treatment type and elastic modulus, suggesting that multiple liberase injections do not affect the nonlinear viscoelasticity of 4T1 tumors.

KEYWORDS

Breast cancer, rheology, drug delivery, mechanotransduction, liberase

INTRODUCTION

Breast cancer is the second leading cause of cancer-related mortalities among women in the US.[1] The American Cancer Society estimates that 290,560 individuals will be newly diagnosed with invasive breast cancer in the United States in 2022 and 43,780 will die as a result of the disease.[2] Triple-negative breast cancers (TNBCs), which lack estrogen receptors, progesterone receptors and excess HER2 protein, make up approximately 15% of all breast tumors.[3] TNBC tumors are highly aggressive and display a significant increase in the number of fibroblasts present, which increase the matrix stiffness through extracellular matrix (ECM) remodeling.[4,5]

The ECM is primarily composed of water and fibrous proteins (such as collagens, fibronectin, laminins, glycosaminoglycans, and proteoglycans), the exact composition of which varies between tissue types and even heterogeneously within the same tissue.[6] The ECM provides structural support by acting as a scaffold to which cells can adhere, while also transmitting the biochemical and biomechanical cues necessary to direct tissue morphogenesis, cellular differentiation, and homeostasis.[6] The most abundant fibrous protein in the ECM is collagen, contributing up to 30% of the total protein mass of a multicellular animal.[6] The role of

collagens in the ECM is to provide tensile strength, regulate cell adhesion, and support chemotaxis and migration.[6,7] The numerous cell types present in the tumor microenvironment (including immune cells, fibroblasts, adipocytes, and microvasculature) and the ECM collectively serve an important role in determining the progression of cancer.[4,7–10]

Physical stimuli can alter cellular signaling pathways through a process called mechanotransduction.[11–13] As the tumor ECM stiffens, cells within the tumor release growth factors in response which promote angiogenesis and increased ECM deposition, leading to a vicious positive-feedback loop of tumor growth.[6,14] The ECM of the mammary gland becomes progressively stiffer during tumor progression due to increased deposition and cross-linking of ECM components such as collagen.[4,10,15] Chemotherapeutic agents are the only Food and Drug Administration-approved agents for treating TNBCs, and more effective therapies are critically needed.[16]

Inhibition of ECM components is a promising therapeutic strategy for breast cancers.[8,15] These approaches have primarily taken the form of inhibiting ECM-remodeling enzymes.[17] For example, Nilsson *et al.*,[18] demonstrated that inhibition of collagen cross-linking enzymes in the lysyl oxidase family led to decreased tumor growth and metastasis. Other studies have attempted

to modify the breast cancer ECM directly using collagenase enzymes as therapeutic agents. Riegler *et al.,*[19] demonstrated that collagenase-D injections reduced the collagen content and stiffness of murine allograft tumors *in vivo* after 24 hours. Pan *et al.*,[20] used co-injections of collagenase-I and trastuzumab (a monoclonal antibody that targets HER2) with a thermosensitive hydrogel system composed of PLGA-PEG-PLGA triblock copolymer to inhibit growth of and induce collagen digestion in HER2-positive xenograft tumors *in vivo*. They observed a four-fold reduction in collagen density, nine-fold reduction in vascular density, and fewer side effects caused by trastuzumab after 28 days.[20]

Many different techniques are used to quantify tissue stiffness, including uniaxial tensile and compressive tests[21] which can be difficult to perform on deformable samples. Nanoindentation[22] and atomic force microscopy[23] provide a high degree of spatial resolution and allow for mapping of tissue heterogeneity, but adhesion between the indenter tip and the sample can interfere with measurements[22] and cause large variations among individual measurements of the same sample.[24] Elastography indirectly evaluates tissue stiffness by measuring the speed of propagating shear waves within the tissue of interest; shear waves travel faster in stiff tissues and slower in soft tissues.[25,26] This assumption limits elastography to utilization only in the linear

viscoelastic regime, in which the shear moduli are constant with respect to the applied strain or deformation.[26]

Rheology is a technique used to characterize the flow and microstructure properties of materials through measurements of mechanical responses to imposed deformations. Two physiologically relevant values, among many, that can be obtained by rheology include the elastic modulus (a measure of strength or stiffness) and viscoelasticity (the relative viscous to elastic nature of the material). The mechanotransductive responses of fibroblasts are affected by both substrate elastic modulus[13,27] and viscoelasticity.[28] Rheological characterization is commonly performed in the small amplitude oscillatory shear (SAOS) regime, in which the total applied deformation is small enough to probe the microstructure without disturbing it. SAOS experiments are used to evaluate a sample's linear viscoelasticity. In contrast, large amplitude oscillatory shear (LAOS) experiments can be used to evaluate the nonlinear viscoelastic material response to large strain amplitudes and deformations, making this a useful technique for measuring tissue properties under physiologically relevant conditions such as tissue injury.[29] Fibrous matrices exhibiting a type of nonlinear elasticity known as strain-stiffening enable cells to transmit forces over distances of up to half a millimeter,[30] facilitating long-range

communication between cells.[31] Strain-stiffening can also lead to directionally persistent tumor invasion in collagen matrices.[32,33] Additionally, matrix nonlinear viscoelasticity influences the shapes assumed by developing solid tumors.[34] SAOS rheology has been used to characterize porcine and murine lungs,[35] collagenase-treated human uterine fibroids,[36,37] and a variety of cancerous tumors in mice,[38] while LAOS has been applied to human skin,[39] bovine livers,[29] and human vocal fold tissues.[40]

In this work, we examine the effects of injectable liberase treatments in the presence or absence of a thermoresponsive copolymer, as well as appropriate controls, on the linear and nonlinear rheological behavior of stage IV, TNBC, 4T1 allograft murine mammary tumors. Liberase is an enzyme blend containing highly purified class I and II collagenases (matrix metalloproteinases which digest both water-insoluble native collagens and water-soluble denatured collagens in the triple helix region, isolated from *Clostridium histolyticum*) and thermolysin (a metallopeptidase that cleaves peptide bonds at the N-terminus of many hydrophobic amino acids, isolated from *Bacillus thermoproteolyticus*).[41–43] In our recent report on quantifying uterine fibroid digestion by co-injected collagenase and LiquoGel (LQG, a thermoresponsive *N*-isopropyl acrylamide-based polymer that transitions upon heating from an

injectable solution to a gel and hydrolyzes over time), we demonstrated that LQG is non-toxic, localizes drug release, and enhances tissue digestion both *ex vivo* and *in vivo* as measured by SAOS rheology and histological staining.[37] We hypothesize that co-injecting LQG will have similar effects here on 4T1 tumors, reducing liberase diffusion from the injection site and allowing for further collagen digestion and tissue softening. An initial *in vivo* mouse study involving a single treatment injection was performed to observe treatment effects on tumor volume and rheology after 3 days. A second *in vivo* study involving five treatment injections over 9 days was then performed to evaluate whether multiple injections enhanced treatment effects over time. Tumors from the first study are subjected to SAOS testing only to evaluate treatment effects on linear viscoelastic behavior, while tumors from the second study undergo both SAOS and LAOS testing to assess whether treatment injections cause deviations in the nonlinear behavior of mammary tumors.

EXPERIMENTAL SECTION

Materials. Tris base (obtained from Sigma Aldrich), sodium chloride (obtained from VWR) and calcium chloride dihydrate (obtained from VWR) were used as received and were combined with deionized (DI) water to prepare the Tris buffer, pH 7.5 (TRIS) containing 109 μM Tris base, 43 μM sodium chloride and 0.3 mg/mL calcium chloride dihydrate. Liberase TL

Research Grade, low thermolysin concentration (Lib) was obtained from Millipore Sigma as a lyophilized powder and was reconstituted in Tris to a stock concentration of 2.5 mg/mL. Matrigel Growth Factor Reduced Basement Membrane Matrix (Matrigel®) was obtained from Corning and used as received. Phosphate-buffered saline, pH 7.4 (PBS) was obtained from ThermoFisher Scientific and diluted to 1x in DI water for use.

LiquoGel (LQG) composition and synthesis. The random tetrameric copolymer LQG was prepared via benzoyl peroxide-initiated free radical copolymerization of individual monomers *N*-isopropylacrylamide (NIPAM, 83%), 2-hydroxyethyl methacrylate conjugated to poly(lactic acid) (HEMA-PLA, 7%), acrylic acid (AAc, 1%), and methacrylated hyperbranched polyglycerol (HPG-MA, 9%) as previously reported.[37,44] Monomer structures are provided in **Figure S1**. NIPAM provides the thermogelling ability, HEMA-PLA adds biodegradability through hydrolysis of side-chain ester bonds, AAc improves water retention within the gel and aids in bioadsorption of the degraded polymer,[45] and HPG-MA provides hydrophilic cavities within the gel for molecular entrapment as well as additional biodegradability through acid-labile acetal linkages.[46] The sol-gel transition of LQG occurs at ~25 °C (**Figure S2**).

Single injection *in vivo* mouse study protocol. All animal experiments were conducted in accordance with the Guidelines for Care and Use of Laboratory Animals of North Carolina Central University and approved by the Institutional Animal Care and Use Committee at North Carolina Central University (NCCU IACUC Protocol No. JF-11-09-2011)**.** 4T1 cells (ATCC, an animal model for stage IV TNBC[47]) were cultured to 80% confluence. $1x10^4$ cells were injected into the right mammary gland of 20 female nude mice in 30 μL of 50% PBS, 50% Matrigel® to induce tumor formation. Matrigel® was included in the injection medium to keep the cells

localized post-injection.[48] Mice were randomly distributed into four treatment groups (5 mice per group). Once the tumors were palpable (designated as day 0), they were injected with 30 μL one of the following treatments: TRIS, Tris (control); TRIS+Lib, 0.01 units of liberase in TRIS; LQG, 15 wt% LQG in TRIS; LQG+Lib, 15 wt% LQG and 0.01 units of liberase in TRIS. The mice were euthanized on day 3, at which point the tumors were harvested and measured by calipers to calculate tumor volume. The tumors were then snap frozen on dry ice and stored at -80 ºC.

Multiple injection *in vivo* mouse study protocol. 4T1 cells were again grown to 80% confluence. $5x10^5$ cells were injected into the right mammary gland of 20 female nude mice in 30 μL of 50% PBS, 50% Matrigel® to induce tumor formation. Mice were randomly distributed into four treatment groups (5 mice per group). The injection buffer was switched from to PBS from TRIS to reduce irritation to the mice. Once the tumors were palpable (designated as day 0), they were injected with 30 μL one of the following treatments: PBS, 1x PBS (control); PBS+Lib, 0.01 units of liberase in PBS; LQG, 15 wt% LQG in PBS; LQG+Lib, 15 wt% LQG and 0.01 units of liberase in PBS. Treatment injections were repeated on days 2, 4, 6, and 9, for a total of five injections. Later on day 9, the tumors were harvested via survival surgery and their volume was measured using calipers. The tumors were then snap frozen on dry ice and stored at -80 ºC. Two mice (one in the PBS group, one in the LQG group) did not survive to day 9 and their tumors were excluded from the study.

Sample preparation for rheology. The tumors were labeled such that the rheological operator was blinded to the identity of the tumor until after all measurements had been conducted. Each tumor was thawed and sliced individually immediately prior to rheological measurement. Repeated cycles of freezing and thawing can decrease tissue modulus and increase

tissue viscoelasticity (as shown for healthy human mammary tissue in **Figure S3**) due to the formation of damaging ice crystals within the tissue,[49] so all 4T1 tumors from the *in vivo* mouse studies were measured on the initial thaw to normalize the samples' thermal history.

Tumors stored at -80 ºC were allowed to partially thaw, from which two ~2 mm thick slices (center and edge) were cut. The center slice was obtained from the widest part of the tumor. Next, ~ 1 mm of tumor tissue was discarded from the larger side remaining from the tumor to evenly space out the two sample locations, and then the edge slice was obtained. Using an 8 mm biopsy punch, a disk of tissue (8 mm in diameter, ~2 mm thick) was finally created from each slice. Both slices were hydrated with a few drops of PBS and brought up to 37 ºC in an incubator, where they equilibrated for 3 minutes. Either the center or edge slice was randomly selected to be measured first on the rheometer, while the other slice remained in the incubator for an additional ~30 min prior to measurement.

Rheological measurement. A Discovery Hybrid Rheometer-3 (DHR-3, TA Instruments) was used for all measurements. The temperature was fixed at 37 ± 0.1 ºC by an Advanced Peltier Plate. To keep the samples hydrated during the measurement, an immersion cell (manufactured by TA Instruments) was secured around the bottom Peltier plate. The bottom and top geometries were both 8 mm crosshatched parallel plates. After loading the tissue onto the rheometer and bringing the top plate down to the specified gap of 1.6 mm, ~40 mL of PBS preheated to 37 ºC was added to the immersion cell until the sample was fully immersed. The gap height was fixed at 1.6 mm for all experiments based on prior work demonstrating that keeping the gap height constant reduced experimental variability,[37] and the axial force at the beginning of the experiment was between 0.03 and 0.05 N. A schematic and picture of the experimental setup (prior to addition of PBS to the immersion cell) are provided in **Figure S4**.

Samples were first allowed to equilibrate at 37 ºC for 2 min. Next, a frequency sweep experiment was performed (ω = 0.01-40 rad/s). The oscillation strain was selected as 0.5%, which was previously determined to be within the linear viscoelastic regime of breast cancer tumors. Samples from the single injection study were only subjected to the frequency sweep experiment, after which they were removed from the rheometer and discarded. Samples from the multiple injection study were subjected to an additional LAOS experiment (γ = 1-40%, ω = 1 rad/s) after a 2 min equilibration period. Between samples, the immersion cell was drained and the plates were dried off in order to ensure good plate contact was made with each tissue. The strain (γ) and shear stress (τ) data from each strain amplitude level were input into the MITlaos MATLAB program[50] for analysis of nonlinear viscoelasticity using the default program settings.

Statistical analysis. All error bars displayed on graphs represent a 95% confidence interval (± 1.96 standard error). Tukey-Kramer honest significant difference (Tukey HSD) tests were performed using JMP Pro 14 (SAS) at a significance level α = 0.05 to simultaneously test all pairwise comparisons among means between treatment groups within each individual study (single or multiple injection).

RESULTS AND DISCUSSION

Single injection study results: tumor volume and linear viscoelasticity. We begin by examining the generic linear viscoelastic behavior of 4T1 mouse mammary tumors. Under SAOS testing conditions, all tumors exhibited gel-like rheological behavior regardless of the imposed treatment, with G' > G" across all frequencies and G' and G" being relatively independent of frequency.[51] Results for two representative tumors are presented below in **Figure**

1. This observed gel-like behavior makes intuitive sense, as ECM components impart solid character to the tissues. Treatment with the matrix-degrading collagenase enzymes contained in liberase can reduce the collagen density and number of collagen crosslinks in the tumor,[52] but does not affect other ECM proteins such as fibronectin or glycosaminoglycans, leaving the solid nature of the tumor intact. Two parameters of interest were selected for analysis of the linear viscoelastic rheological data to compare between treatment groups. The elastic modulus (G') at frequency ω = 1 rad/s was chosen as the measure for tissue modulus, while the value of tan δ (defined as $\equiv$ G"/G') was used to evaluate tissue viscoelasticity at the same frequency ω = 1 rad/s.

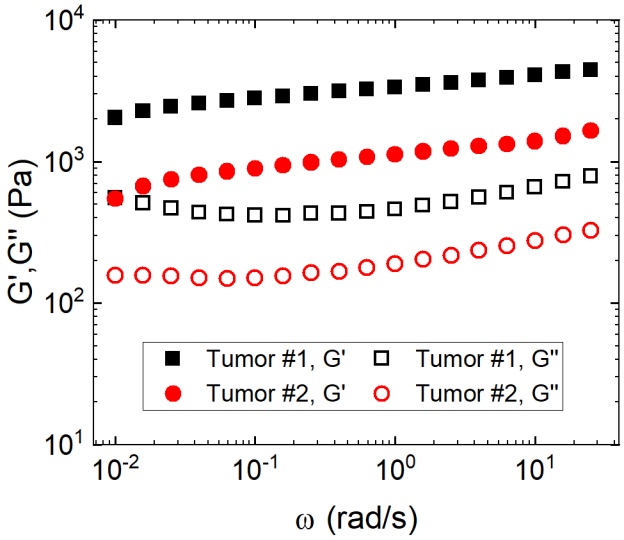

Figure 1. Frequency sweep data for two representative tumor samples (labeled as Tumor #1 and Tumor #2), both of which exhibit gel-like rheological behavior.

The effects of a single treatment injection after 3 days of *in vivo* incubation are shown in **Figure 2**, while images of representative tumors are given in **Figure S5**. The tumor volume data presented in **Figure 2a** illustrates that the TRIS-treated tumors had the highest average final tumor volume (1350 ± 350 mm^3) compared to the other treatment groups. TRIS+Lib reduced the final tumor volume to 861 ± 269 mm^3. LQG had little effect on the final tumor volume (1220 ± 690 mm^3) compared to the TRIS buffer control. The localized injection treatment of LQG+Lib caused the largest decrease in final tumor volume to 434 ± 325 mm^3, and this difference was statistically significant compared to the TRIS buffer control group ($p = 0.0467$).

The tissue modulus data presented in **Figure 2b** reveal that the tissue modulus for tumors injected with the TRIS buffer control was slightly higher at the edge (2520 ± 590 Pa) than at the center (1490 ± 245 Pa). This same trend holds for the tumors injected with TRIS+Lib, where the tissue modulus at the edge (1840 ± 465 Pa) was somewhat higher than at the center (1530 ± 442 Pa). Comparing TRIS with TRIS+Lib, the effect of a single free liberase injection on tissue modulus appears minimal. For LQG-treated tumors, the tissue modulus at the center (1910 ± 1000 Pa) is slightly higher than that at the edge (1670 ± 587 Pa). Tumors treated with LQG+Lib displayed the lowest tissue moduli at both the center (1210 ± 406 Pa) and edge (1070 ± 264 Pa), suggesting that a single localized collagenase injection acts to soften 4T1 breast cancer tumors. The reduction in tissue modulus was statistically significant for LQG+Lib center vs. TRIS edge ($p = 0.044$) and LQG+Lib edge vs. TRIS edge ($p = 0.018$). Numerical simulations of poroelastic tissues demonstrate that the shear modulus decreases with increasing tissue porosity;[53] thus, we would expect tumors treated with a single injection of LQG+Lib to be the most porous, potentially allowing for increased diffusion of chemotherapeutic drugs into the tumor.[54] The slightly higher observed G' values at the tumor center compared to the edge for LQG and

LQG+Lib could perhaps be due to LQG polymer remaining concentrated at the tumor center; however, the amount of polymer injected was quite low (~ 7.5 μg), so we expect that these differences are more likely due to experimental variability.

The tissue viscoelasticity data presented in **Figure 2c** yielded no statistically significant differences between treatment groups. However, it does demonstrate that for all treatment groups, the average tissue viscoelasticity (tan δ) was slightly higher at the tumor center compared to the edge, and that treatment appears to have no discernible effect on tan δ. Differences in tan δ between the tumor center and edge slices reflect the 4T1 tumor morphology; as the tumors rapidly grow outwards, an inner necrotic core develops, while proliferating cells (which continue to deposit ECM) remain on the outer edge.[55] Thus, the somewhat higher tan δ values at the tumor centers possibly reflect the increased viscous nature of the necrotic core.

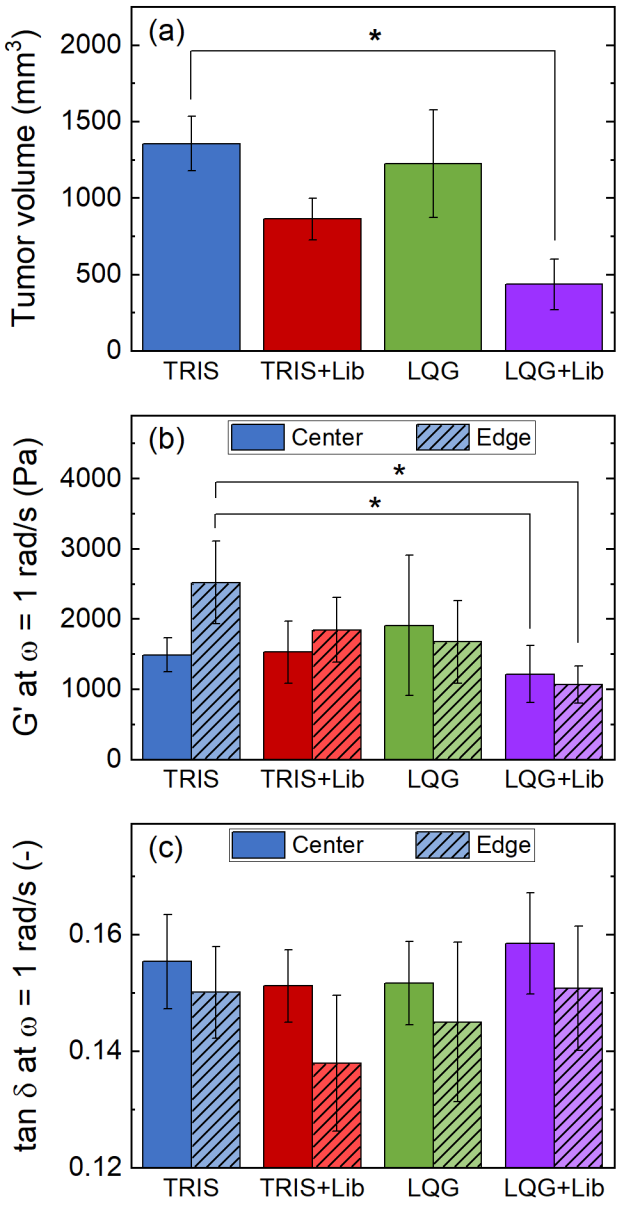

Figure 2. Effect of single injection treatment on (a) final tumor volume, (b) tissue modulus (G' at ω = 1 rad/s) and (c) tissue viscoelasticity (tan δ at ω = 1 rad/s), split by location of tissue slice (center vs. edge). Significance level of * denotes $p < 0.05$.

Overall, the results from the single injection study suggest that LQG+Lib may be a promising treatment to reduce the size and mechanical strength (G') of 4T1 tumors without

affecting tissue viscoelasticity. We hypothesized that injecting the tumors multiple times with LQG+Lib could induce a more dramatic response. In the next section, we explore how 4T1 tumors responded to repeated treatment injections.

Multiple injection study results: tumor volume and linear viscoelasticity. The effects of multiple treatment injections over 9 days of *in vivo* incubation are presented in **Figure 3**. No statistically significant differences between treatment groups were observed in any of the response variables. The tumor volume data presented in **Figure 3a** shows that the two control injection groups (PBS and LQG) once again had the highest average final tumor volume (1440 ± 761 mm^3 for PBS, and 1610 ± 1240 mm^3 for LQG) compared to the other treatment groups. PBS+Lib slightly reduced the final tumor volume to 870 ± 479 mm^3, while the localized injection treatment of LQG+Lib caused the largest decrease in final tumor volume to 302 ± 166 mm^3. As noted above, the difference in tumor volume between PBS and LQG+Lib was not statistically significant in this study ($p = 0.090$).

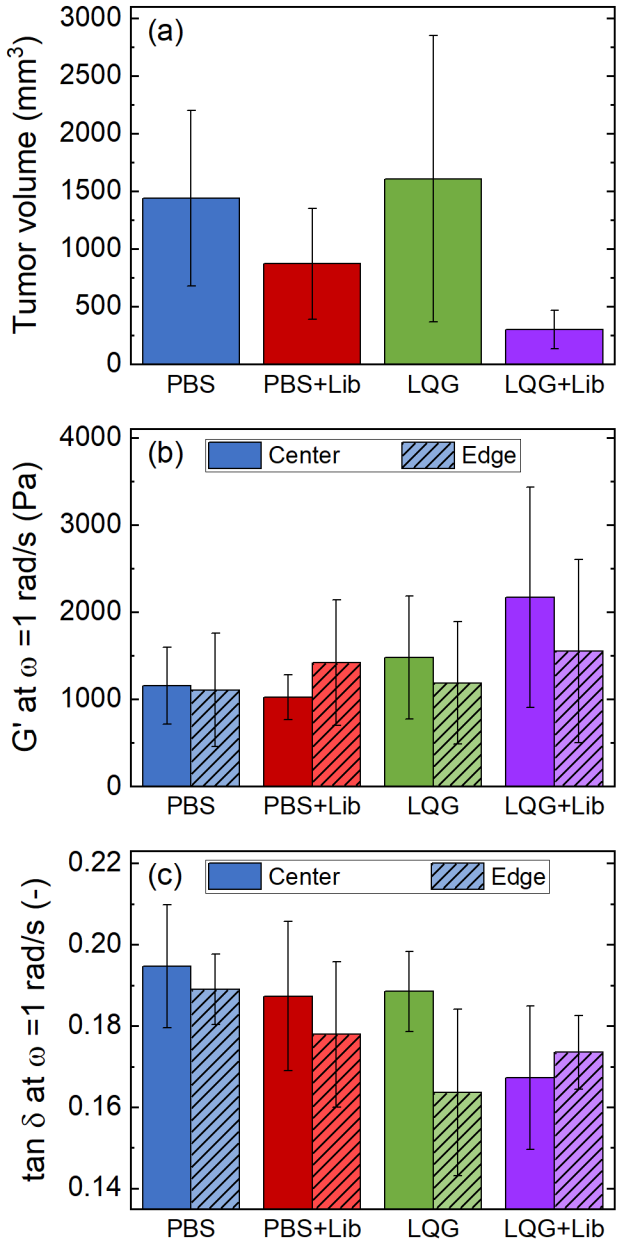

Figure 3. Effect of multiple injection treatment on (a) final tumor volume, (b) tissue modulus (G' at ω = 1 rad/s) and (c) tissue viscoelasticity (tan δ at ω = 1 rad/s), split by location of tissue slice (center vs. edge).

The tissue modulus data for the multiple injection study is presented in **Figure 3b**. The tissue modulus for PBS-injected tumors was nearly equal at the center (1160 ± 438 Pa) and at the edge (1110 ± 650 Pa). For PBS+Lib, the tissue modulus at the edge (1420 ± 718 Pa) was somewhat higher than at the center (1023 ± 256 Pa). Direct comparison of PBS with PBS+Lib reveals that multiple free liberase injections did not have a more pronounced softening effect. In a similar fashion to the single injection study, LQG-injected tumors had a slightly higher tissue modulus at the center (1480 ± 706 Pa) than that at the edge (1190 ± 701 Pa). However, in stark contrast to the single injection study, LQG+Lib had the highest tissue modulus at both the center (2170 ± 1260 Pa) and edge (1550 ± 1050 Pa), though this increase in tissue modulus was not statistically significant ($p > 0.05$ compared to all other treatment groups). **Figure 3c** demonstrates that LQG+Lib causes the lowest observed tissue viscoelasticity at the tumor center, and that LQG+Lib tumors were slightly more viscoelastic at the tumor edge than at the center. For the other three treatment groups, the average tissue viscoelasticity was higher at the tumor center compared to the edge, matching the trend established in **Figure 2c**.

The data presented in **Figures 3b-c** appear counterintuitive, as one would expect that repeated enzymatic injections would act to soften, not stiffen, tumors. We postulate that the trends of final tumor volume, tissue modulus, and tissue viscoelasticity from **Figure 3** can be related through a mechanotransductive mechanism. A schematic detailing this possible mechanism is presented in **Figure 4**. Tumors treated with PBS (**Figure 4a**) contain a stiff microenvironment, which induces an invasive cellular phenotype and promotes outward tumor growth. As the tumors grow larger, ECM (purple lines) deposition occurs evenly throughout the tumor, leading to similar modulus values obtained at the center versus the edge of the tumors. In contrast, the local tumor microenvironment is softened by treatment with LQG+Lib (**Figure 4**),

which discourages outward growth and leads to the formation of smaller tumors. Cells concentrated at the center of the tumor deposit ECM locally, leading to higher G' and lower tan δ values observed at the center compared to the edge of the tumors. While no drastic differences in ECM distribution were observed between treatment groups in hematoxylin and eosin (H&E) stains of representative tumors (**Figure S6**), the ECM components (stained by H&E in varying degrees of pink, while nuclei are stained blue) appear to be packed slightly more densely for PBS+Lib and LQG+Lib compared to PBS and LQG.

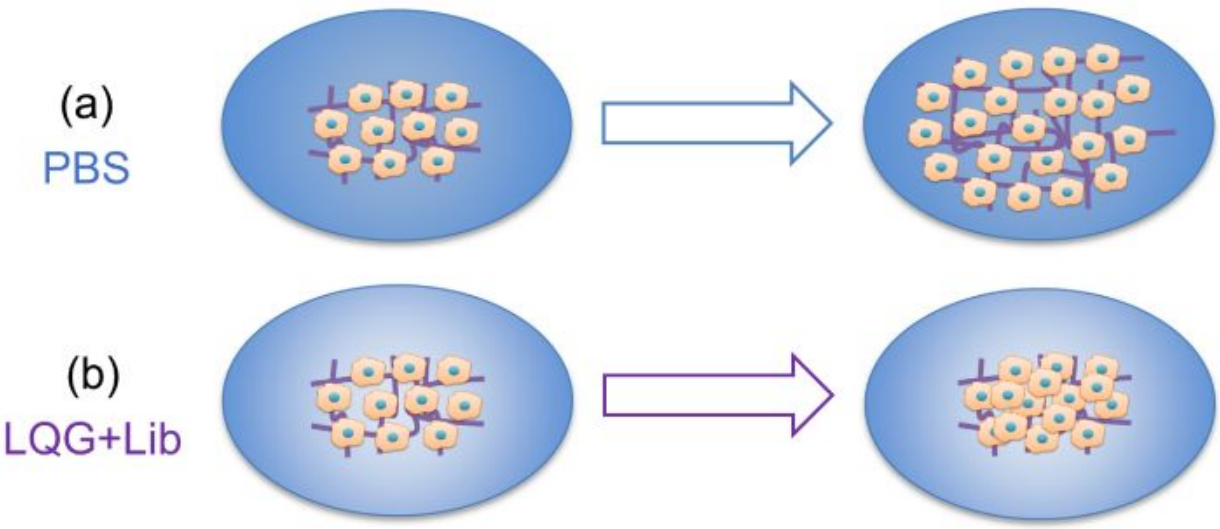

Figure 4. Schematic explaining how the tumor volume and modulus trends (Figures 3a-b) may be related through mechanotransduction.

As no statistically significant differences between treatment groups were observed in the multiple injection study, repeat studies containing more tumor replicates will be needed to validate these results. In an attempt to elucidate more distinctions between the treated and

untreated 4T1 tumors in the multiple injection study, we turn to LAOS analysis of tumor nonlinear viscoelasticity.

Multiple injection study results: MITlaos analysis of nonlinear viscoelasticity. Upon moving from the linear to the nonlinear regime by increasing to large strain amplitudes, the linear viscoelastic parameters G' and G" become no longer suitable for describing a sample since the nonlinear stress response is not a single harmonic sinusoid.[50] To interpret these higher harmonics in a physically meaningful matter, Ewoldt *et al.*,[50] expanded upon the concept of orthogonal decomposition introduced by Cho *et al.*,[56] and used Chebyshev polynomials to describe the elastic (σ') and viscous (σ") stress responses as follows:

$$\sigma' = \gamma_0 \sum_{n:odd} e_n(\omega,\gamma_0) T_n(\frac{\gamma}{\gamma_0}) \quad (1)$$

$$\sigma'' = \dot{\gamma}_0 \sum_{n:odd} v_n(\omega,\gamma_0) T_n(\frac{\dot{\gamma}}{\dot{\gamma}_0}) \quad (2)$$

where γ is the imposed strain, γ_0 is the strain amplitude (largest imposed strain in each oscillatory cycle), $\dot{\gamma}$ is the strain rate, $\dot{\gamma}_0$ is the strain rate amplitude, and T_n is the *n*th-order Chebyshev polynomial of the first kind.[50] The two quantities e_n and v_n are the elastic and viscous Chebyshev coefficients and are given by:

$$e_n = G'_n(-1)^{\frac{n-1}{2}} \quad (3)$$

$$v_n = \frac{G''_n}{\omega} \quad (4)$$

where G'_n and G''_n are the *n*th-order elastic and viscous moduli, respectively. In the linear regime, e_3/e_1 and $v_3/v_1 << 1$, and Equations 3 and 4 collapse back to the linear viscoelastic result such that $e_1 \rightarrow G'$ and $v_1 \rightarrow G''/\omega$.[50]

Two additional definitions of elastic moduli are introduced:

$$G'_M = \left.\frac{\partial\sigma}{\partial\gamma}\right|_{\gamma=0} = e_1 - 3e_3 + \ldots \quad (5)$$

$$G'_L = \left.\frac{\partial\sigma}{\partial\gamma}\right|_{\gamma=\pm\gamma_0} = e_1 + e_3 + \ldots \quad (6)$$

where G'_M is the elastic modulus at the minimum (zero) strain and G'_L is elastic modulus at the largest imposed strain, and e_1 and e_3 are the first and third order elastic Chebyshev coefficients, respectively. Both G'_M and G'_L are intercycle quantities, meaning they occur across cycles of different maximum observed strain values. Similarly, to capture the viscous nature of the material, the following definitions of dynamic viscosities are introduced:

$$\eta'_M = \left.\frac{\partial\sigma}{\partial\dot{\gamma}}\right|_{\dot{\gamma}=0} = v_1 - 3v_3 + \ldots \quad (7)$$

$$\eta'_L = \left.\frac{\partial\sigma}{\partial\dot{\gamma}}\right|_{\dot{\gamma}=\pm\dot{\gamma}_0} = v_1 + v_3 + \ldots \quad (8)$$

where η'_M is the dynamic viscosity at minimum (zero) strain rate and η'_L is the dynamic viscosity at the largest imposed strain rate. These quantities are illustrated on plots of the raw stress vs. strain (also called Lissajous-Bowditch curves) in **Figure 5**. At low strain amplitudes within the linear viscoelastic regime, the elastic and viscous Lissajous-Bowditch curves (**Figures 5a**, **c**) are undistorted, and $G'_M = G'_L$ and $\eta'_M = \eta'_L$. As the strain amplitude is increased into the nonlinear viscoelastic regime, the shapes of the elastic and viscous Lissajous-Bowditch curves become distorted (**Figures 5b, d**) and the elastic moduli and dynamic viscosities deviate from each other.

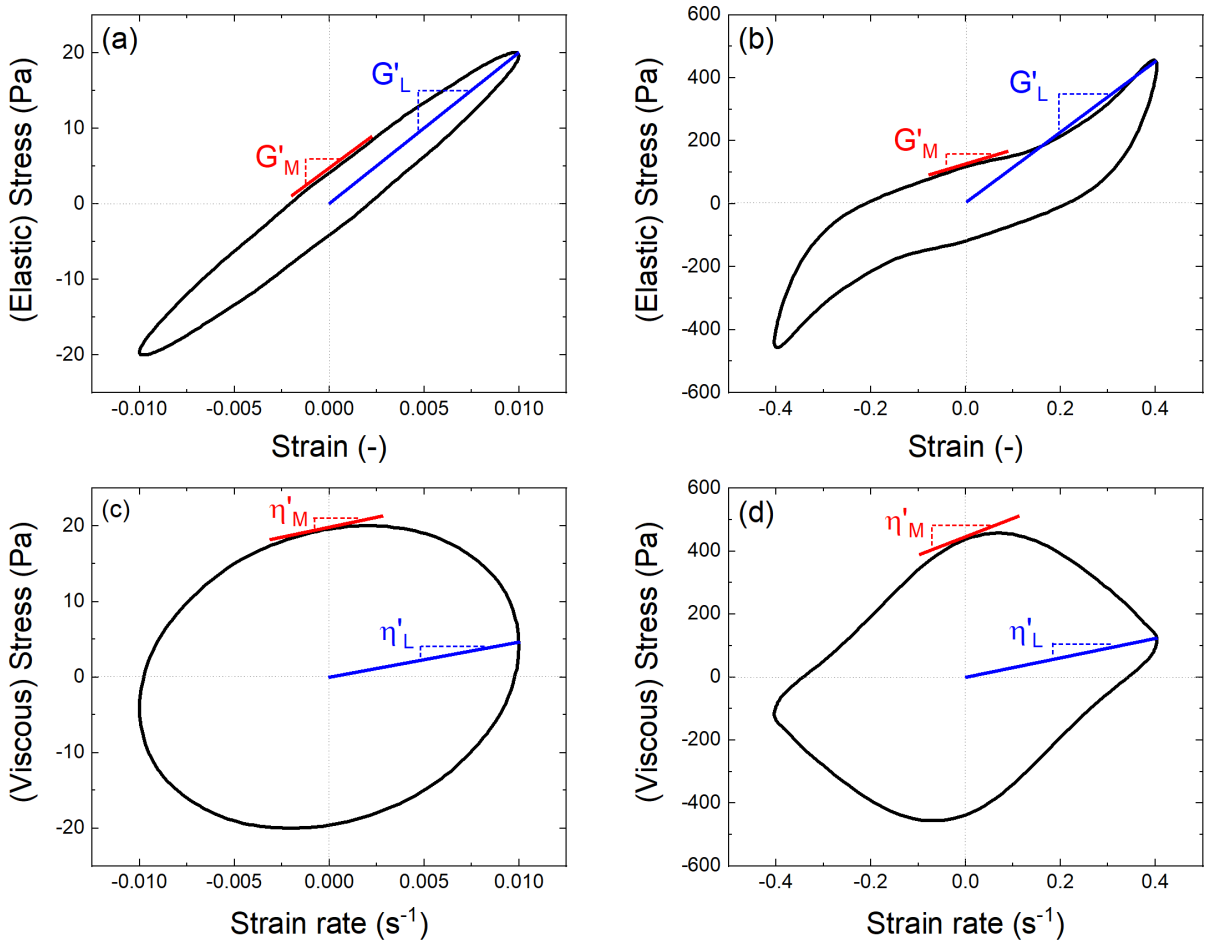

Figure 5. Example elastic (a, b) and viscous (c, d) Lissajous-Bowditch curves, illustrating the definitions of the intercycle storage moduli (G'_M and G'_L) and the intercycle coefficients of viscous dissipation (η'_M and η'_L). The undistorted curve shapes in (a) and (c) indicate linear viscoelastic responses, while the distorted shapes in (b) and (d) indicate nonlinear viscoelastic responses. Figure adapted from Ewoldt *et al.*,[50] and Chan.[40]

LAOS experiments are typically performed over a range of both strain amplitudes and oscillatory frequencies; however, due to our experimental design, we were limited with regard to the accessible frequency range. Frequencies below 1 rad/s could not be explored without

increasing the total experiment time to over 1 hour, and we sought to avoid long experiments to prevent sample aging. At frequencies above 5 rad/s, inertial effects resulting from the small (8 mm diameter) parallel plates used with a commercial rheometer overwhelmed the torque signal, leading to low quality data. Within the range of frequencies ω = 1-5 rad/s, initial screening (data not shown) suggested that nonlinear viscoelastic measures were relatively independent of frequency, so we have chosen to report data at only a constant frequency of 1 rad/s. Additionally, because no significant differences in linear viscoelasticity were observed between center and edge slices from the multiple injection study, data for the center and edge slices have been combined into a single data set for analysis of nonlinear viscoelasticity.

We begin our LAOS analysis of the multiple injection treatment study data by first examining the transition from linear to nonlinear behavior using representative elastic and viscous Lissajous-Bowditch curves at three different strain and strain rate amplitudes, presented in **Figures 6** and **7** respectively. At 1% strain and a strain rate of 0.01 s^{-1}, all treatment groups exhibit linear elastic and viscous behavior, as evidenced by undistorted Lissajous-Bowditch curves that resemble those in **Figures 5a, c**. At 10% strain and a strain rate of 0.1 s^{-1}, minimal deviations from linear elastic behavior are evident (**Figure 6**) while distortions begin to appear in the viscous responses (**Figure 7**). At the maximum imposed strain of 40% and strain rate of 0.4 s^{-1}, both the elastic and viscous Lissajous-Bowditch curves take on pronounced distorted shapes resembling those in **Figures 5b, d**. No differences are visually observed between treatment groups in either the elastic or viscous tissue responses, as the curve shapes are similar across all treatment groups at a designated strain level.

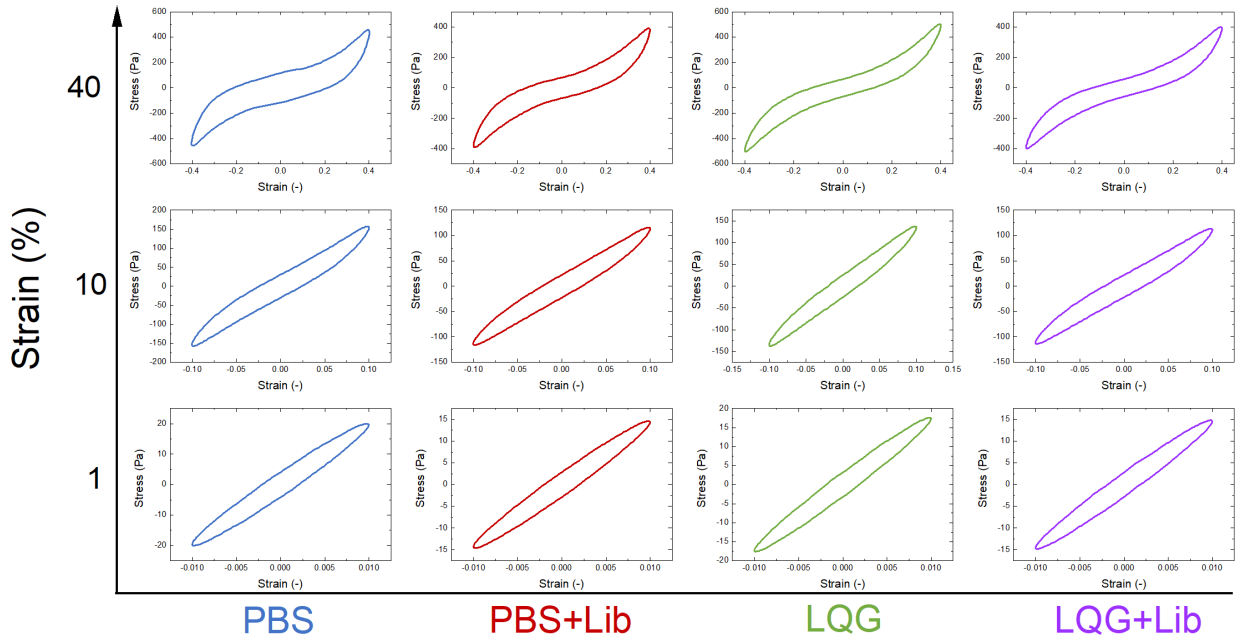

Figure 6. Representative elastic Lissajous-Bowditch curves (stress vs. strain) obtained at frequency ω = 1 rad/s for multiple injection-treated tumors.

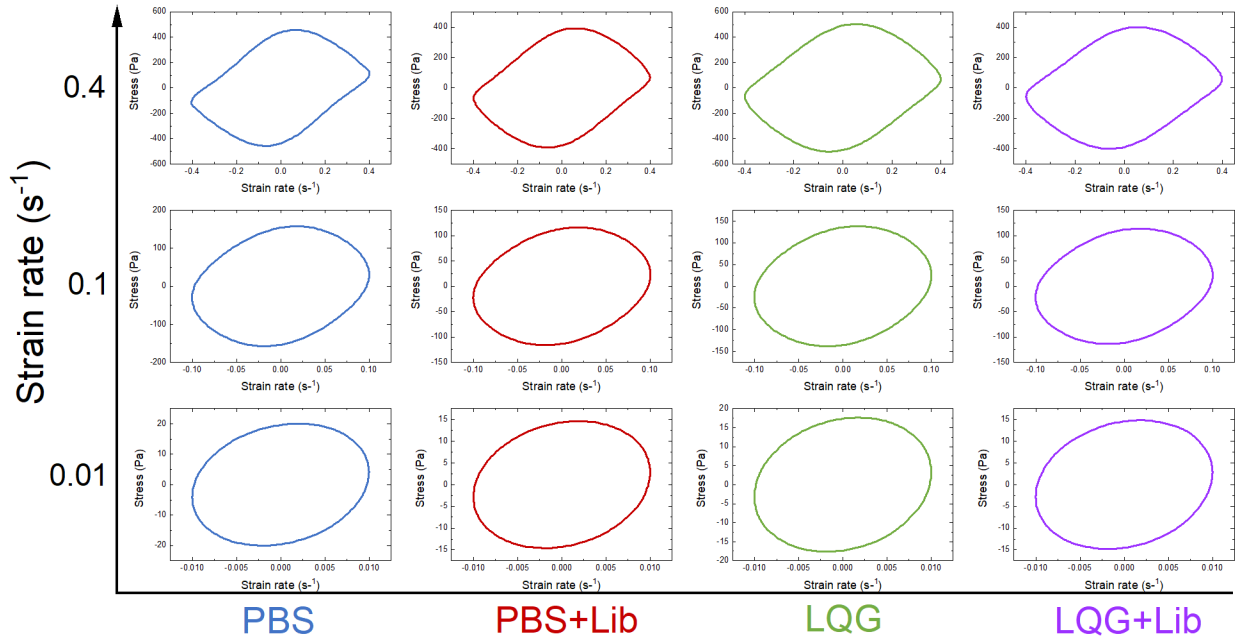

Figure 7. Representative viscous Lissajous-Bowditch curves (stress vs strain rate) obtained at frequency ω = 1 rad/s for multiple injection-treated tumors.

Analysis of the Chebyshev coefficients at higher harmonics (n = 3 and above) allows for physical interpretation of the nonlinear viscoelastic behavior. Intracycle (occurring within a single stress-strain curve cycle) strain-stiffening occurs when $e_3/e_1 > 0$ and strain-softening occurs when $e_3/e_1 < 0$. Similarly, a material has intracycle shear-thickening behavior when $v_3/v_1 > 0$ and has shear-thinning behavior when $v_3/v_1 < 0$.[40,50] **Figure 8** depicts how the elastic and viscous Chebyshev coefficient ratios vary with imposed strain and strain rate for each treatment group.

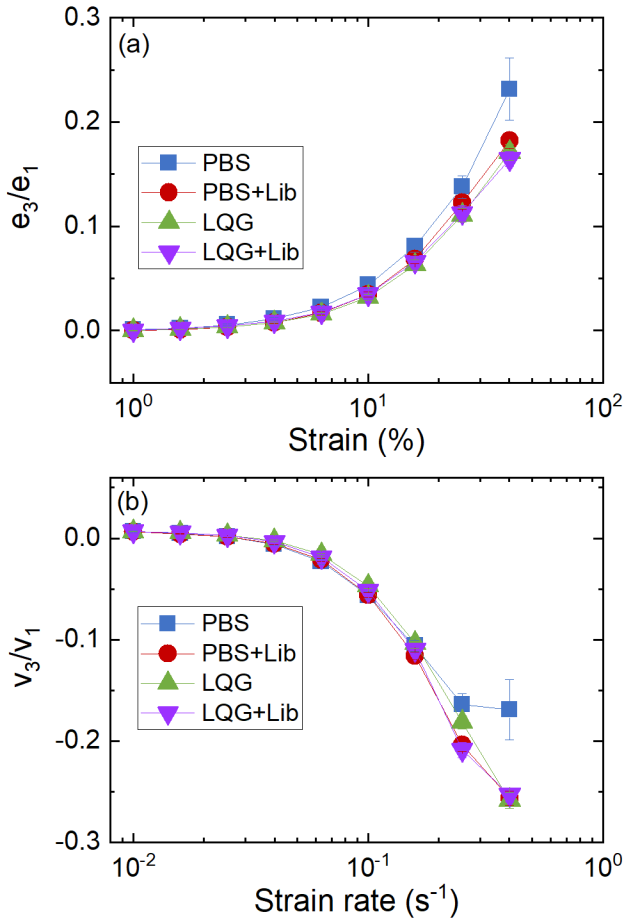

Figure 8. (a) Effect of the multiple injection treatments on (a) intracycle elastic Chebyshev coefficients (e_3/e_1) and (b) intracycle viscous Chebyshev coefficients (v_3/v_1).

We observe that tumor samples subjected to all four treatment types display linear behavior (e_3/e_1 and $v_3/v_1 \sim 0$) up to strains of 5% and strain rates of 0.05 s^{-1}. Above that point, all samples begin to exhibit intracycle strain-stiffening ($e_3/e_1 > 0$) and shear-thinning ($v_3/v_1 < 0$) behavior. As expected, and in accordance with **Figures 6-7**, the degree of nonlinearity increases with increasing strain as the Chebyshev coefficient ratios reach higher absolute values. The data for PBS deviates slightly from that of the other three treatment groups (PBS+Lib, LQG, and LQG+Lib) at high strains (> 25%) and strain rates (> 0.25 s^{-1}); PBS samples appear to be more strain-stiffening and less shear-thinning than the other samples. This result is not entirely expected, as the linear elastic moduli and viscoelasticity values for PBS (**Figures 3b-c**) are very close to that of PBS+Lib and LQG. Indeed, based on the linear viscoelastic data, we might have expected the LQG+Lib data to deviate from the other treatment groups, but such was not the case. Perhaps the mere presence of injected material (LQG polymer and/or Lib enzyme) is responsible for the decreased strain-stiffening and increased shear-thinning behaviors observed. Lim *et al.,*[57] demonstrated for polymer nanocomposites that nonlinear viscoelastic properties increased with particle concentration and were sensitive to the internal microstructure of heterogeneous systems; LAOS experiments conducted on tumors injected with varying LQG and Lib levels could test this whether a similar dependence on the amount of injected material is observed in our systems.

As mentioned previously, the transition from linear to nonlinear behavior can be evidenced in multiple ways, including distortions in the Lissajous-Bowditch curves, deviations in the Chebyshev coefficient ratios from zero, and by deviations in the elastic moduli and dynamic viscosities from their linear counterparts. Information about both intercycle and intracycle nonlinear behavior can be gleaned from elastic modulus and dynamic viscosity data. If G'_L and

G'_M both increase with increasing strain, this is indicative of intercycle strain-stiffening, while intercycle strain-softening is evidenced by G'_L and G'_M both decreasing with increasing strain. Likewise, if η'_L and η'_M both increase with increasing strain rate, that indicates intercycle shear-thickening, while intercycle shear-thinning is evidenced by η'_L and η'_M both decreasing with increasing strain rate. Intracycle strain-stiffening occurs when $G'_L > G'_M$ at a single strain amplitude, while intracycle strain-softening occurs for $G'_L < G'_M$. Correspondingly, intracycle shear-thickening occurs when $\eta'_L > \eta'_M$ at a single strain amplitude, while intracycle shear-thinning occurs for $\eta'_L < \eta'_M$.[40,50]

We observe from the elastic modulus data in the left column of **Figure 9** that tissues in all treatment groups display linear elastic behavior up to strains of ~10%, above which G'_L and G'_M begin to deviate from their linear counterpart (G'_1). This transition point is slightly higher than that identified from analysis of **Figure 8a** (5% strain), suggesting that the elastic Chebyshev coefficients may be a more sensitive measure of nonlinearity than the elastic moduli. We also observe that irrespective of treatment type, all tissues exhibit intercycle strain-softening and intracycle strain-stiffening behaviors. The trend of intracycle strain-stiffening is in agreement with that previously identified from **Figure 8a**. The G'_L data in **Figure 9a** for PBS shows a slight increase from 15% to 25% strain, but then G'_L goes back down for 40% strain. This indicates that PBS-injected tumors exhibit more complex nonlinear behavior than the other tumors, with a slight amount of intercycle strain-stiffening observed at 25% strain.

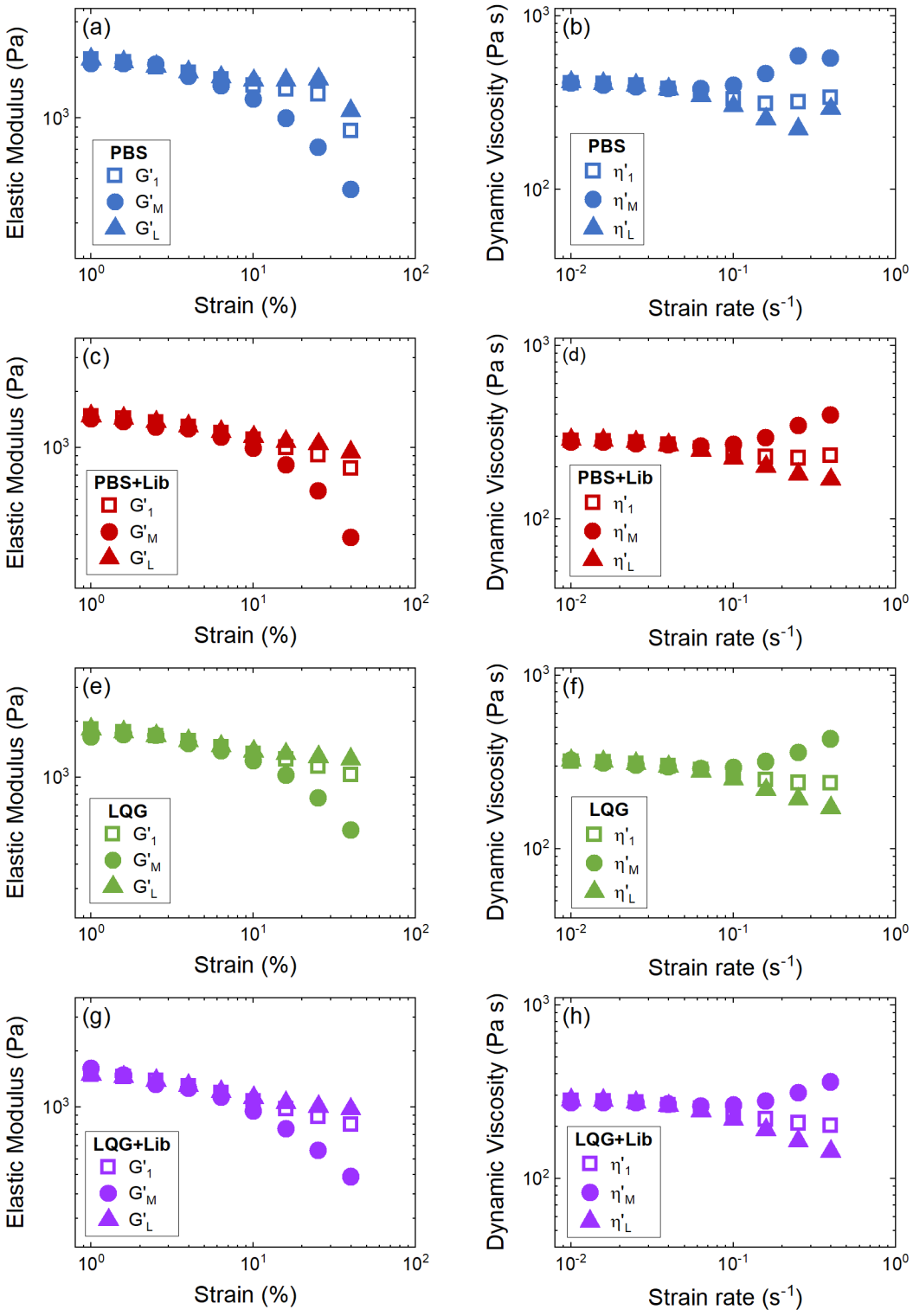

Figure 9. Dependence of elastic moduli and dynamic viscosities on imposed strain and strain rate for PBS (a, b), PBS+Lib (c, d), LQG (e, f), and LQG+Lib (g, h).

We next turn our attention to the dynamic viscosity data presented in the right column of **Figure 9**. Nonlinear behavior is observed across all treatment groups for strain rates above 0.1 s^{-1}, which is again slightly higher than the threshold value of 0.05 s^{-1} identified in **Figure 8b**. Interpretation of the intercycle behavior proves more difficult; η'_M increases with increasing strain rate, while η'_L decreases with increasing strain rate. This data is similar to that obtained for gastropod pedal mucus.[50] Looking instead at η'_1, which can be interpreted as an average of the two other dynamic viscosity quantities, we note that LQG and LQG+Lib exhibit a slight amount of intercycle shear-thinning, while PBS and PBS+Lib exhibit intercycle shear-thinning up to strain rates of 0.25 s^{-1} but then shear-thicken at 0.4 s^{-1}. From this, we can infer that the presence of LQG is associated with intercycle shear-thinning, while a lack of LQG is associated with intercycle shear-thickening at the highest strain rates explored. The intracycle behavior is clearly shear-thinning for all treatment groups ($\eta'_L < \eta'_M$), again matching the conclusion drawn from **Figure 8b**. Deviations from the trends established for other treatment groups are observed for PBS in **Figure 9b**, this time at 0.4 s^{-1}, at which η'_L increases and η'_M decreases from the previous data points. This observation again suggests that 4T1 tumors injected with the buffer control (PBS) exhibit more complex nonlinear behaviors.

Finally, we examined whether a sample's nonlinear behavior was related to its linear elastic modulus, independent of treatment group. The tumor slices were sorted into four quartiles based on their elastic modulus, and data for the lower and upper quartiles is presented in **Figure 10**.

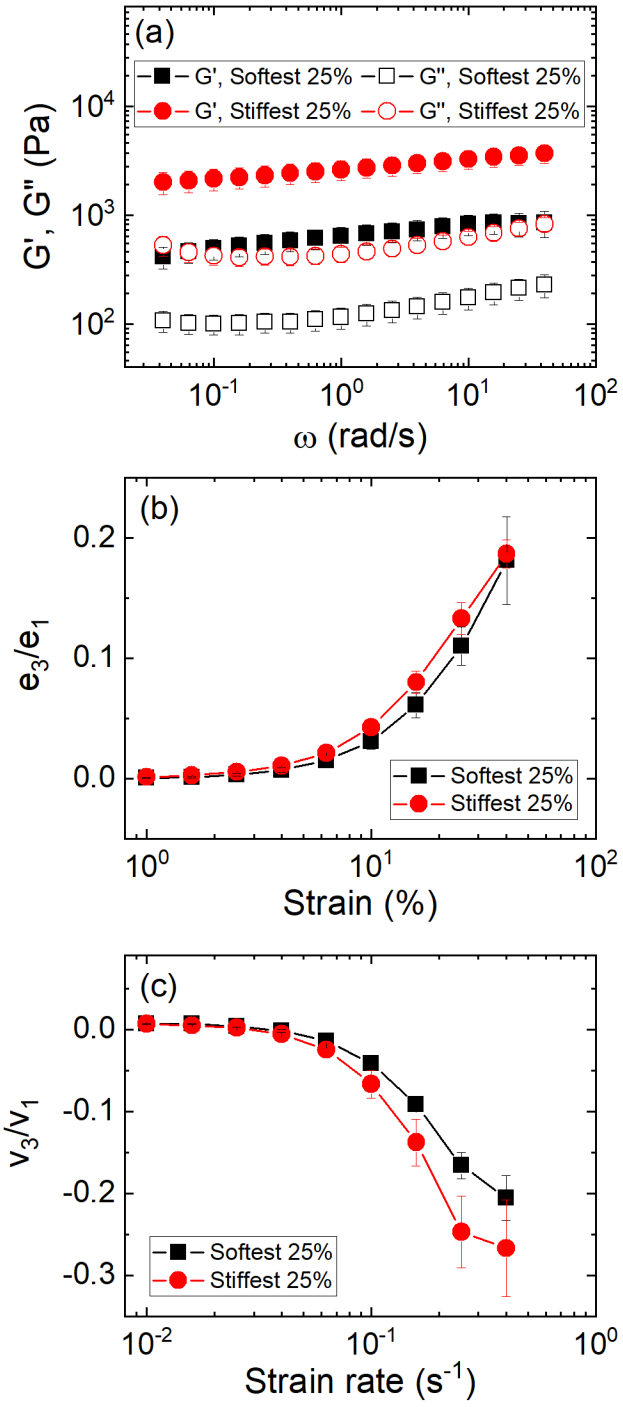

Figure 10. (a) Average elastic (G') and viscous (G") moduli for the tumor slices in the bottom quartile (softest 25%) and top quartile (stiffest 25%). (b) Effect of tissue modulus (softest and stiffest 25%) on intracycle elastic Chebyshev coefficient ratios (e_3/e_1). (c) Effect of tissue modulus on intracycle viscous Chebyshev coefficient ratios (v_3/v_1).

The softest and stiffest 25% of tumors are distinguishably different in their elastic and viscous moduli (**Figure 10a**); however, virtually no difference is observed in the elastic Chebyshev coefficient ratios between these two quartiles (**Figure 10b**), and both quartiles exhibit intracycle strain-stiffening behavior. The viscous Chebyshev coefficient ratios (**Figure 10c**) reveal that stiffest 25% of tumors exhibited a higher degree of intracycle shear-thinning than the softest 25%. We conclude that the onset of nonlinearity is similar for all 4T1 tumors, independent of elastic modulus as well as treatment.

Throughout our LAOS analysis of the 4T1 mammary tumors from the multiple injection study, we observed that treatment type had little-to-no effect on nonlinear behavior. This suggests that the enzymatic treatments did not change the fundamental nature of the breast cancer tissue, and that nonlinear behavior is dictated by ECM components that were unaffected by liberase treatments (such as fibronectin or glycosaminoglycans). Perhaps by increasing the amount of injected enzyme or switching to a blend of collagenase enzymes with greater activity, larger differences in nonlinear behavior could be elucidated. Further exploration could also reveal whether tumor ECM degradation via localized enzymatic injections can enhance the effectiveness of co-injected chemotherapeutic agents, with the overall goal of developing new therapies for metastatic TNBCs.

CONCLUSIONS

We examined how two sets of injectable liberase treatments affected the linear and nonlinear rheological behavior of 4T1 mammary tumors. All tissue samples explored in this work exhibited gel-like rheological behavior in the linear regime. We observed in the single injection study that after 3 days, tumors injected with localized liberase (LQG+Lib) had significantly smaller tumor volumes and lower tissue moduli at both the center and edge compared to buffer- and free liberase-injected control tumors, while tissue viscoelasticity remained relatively unaffected. A contrasting trend in tissue modulus was observed in the multiple injection study; while LQG+Lib tumors remained the smallest in volume, they had higher tissue moduli and lower viscoelasticities compared to the other treatment groups. We postulate a mechanotransductive mechanism to explain these linear rheological results, by which the tumor microenvironment is softened by treatment with LQG+Lib and discourages outward growth, leading to the development of smaller and stiffer tumors. LAOS analysis revealed that all 4T1 tumors from the multiple injection study exhibit nonlinear rheological behavior at high strains and strain rates. Examination of the Lissajous-Bowditch curves, Chebyshev coefficient ratios, elastic moduli, and dynamic viscosities demonstrated that the onset and type of nonlinear behavior was independent of treatment type and elastic modulus, suggesting that the multiple liberase injections did not affect underlying tissue mechanics and that the nonlinear viscoelasticity of 4T1 tumors is dictated by ECM components that were unaffected by liberase treatments. Continued investigation will examine whether increasing the enzyme amount or activity could yield greater changes in linear and/or nonlinear rheological behavior.

This work demonstrates how rheology can be used to characterize tumors that have been treated with matrix-digesting enzymes and the types of insights about the tumor

microenvironment that can be gleaned from the rheological data. The combination of ECM-degrading enzymes with injectable *in situ* forming hydrogel drug delivery systems show great promise in treating early stage cancers.[15] Our results have implications for the design and use of polymeric biomaterials in ECM-remodeling therapies for solid tumors and illustrate how interactions between polymers, enzymes, and cancer cells affect tissue biomechanics in both the linear and nonlinear regimes.

CONFLICTS OF INTEREST

This work was prepared while Jodie Fleming was employed at North Carolina Central University. The opinions expressed in this article are the author's own and do not reflect the view of the National Institutes of Health, the Department of Health and Human Services, or the United States government.

ACKNOWLEDGEMENTS

This work was supported by the National Cancer Institute of the National Institutes of Health under award number 1R15CA223994-01A1. R.D.C. gratefully acknowledges support from the NSF Graduate Research Fellowship and the GAANN Fellowship in Molecular Biotechnology. The authors also thank Lindsey Constantini for assistance with imaging the H&E stains and Randy Ewoldt for providing the MITlaos software.

REFERENCES

1 H. Sung, J. Ferlay, R. L. Siegel, M. Laversanne, I. Soerjomataram, A. Jemal and F. Bray, *CA. Cancer J. Clin.*, 2021, **71**, 209–249.

2 R. L. Siegel, K. D. Miller, H. E. Fuchs and A. Jemal, *CA. Cancer J. Clin.*, 2022, **72**, 7–33.

3 C. Denkert, C. Liedtke, A. Tutt and G. von Minckwitz, *The Lancet*, 2017, **389**, 2430–2442.

4 S. Kaushik, M. W. Pickup and V. M. Weaver, *Cancer Metastasis Rev.*, 2016, **35**, 655–667.

5 I. Acerbi, L. Cassereau, I. Dean, Q. Shi, A. Au, C. Park, Y. Y. Chen, J. Liphardt, E. S. Hwang and V. M. Weaver, *Integr. Biol.*, 2015, **7**, 1120–1134.

6 C. Frantz, K. M. Stewart and V. M. Weaver, *J. Cell Sci.*, 2010, **123**, 4195–4200.

7 T. Rozario and D. W. DeSimone, *Dev. Biol.*, 2010, **341**, 126–140.

8 J. Insua-Rodríguez and T. Oskarsson, *Adv. Drug Deliv. Rev.*, 2016, **97**, 41–55.

9 P. Lu, K. Takai, V. M. Weaver and Z. Werb, *Cold Spring Harb. Perspect. Biol.*, 2011, **3**, a005058.

10 T. R. Cox, *Nat. Rev. Cancer*, 2021, **21**, 217–238.

11 E. K. Paluch, C. M. Nelson, N. Biais, B. Fabry, J. Moeller, B. L. Pruitt, C. Wollnik, G. Kudryasheva, F. Rehfeldt and W. Federle, *BMC Biol.*, 2015, **13**, 47–60.

12 F. Broders-Bondon, T. H. Nguyen Ho-Bouldoires, M.-E. Fernandez-Sanchez and E. Farge, *J. Cell Biol.*, 2018, **217**, 1571–1587.

13 K. Dey, E. Roca, G. Ramorino and L. Sartore, *Biomater. Sci.*, 2020, **8**, 7033–7081.

14 F. Bordeleau, B. N. Mason, E. M. Lollis, M. Mazzola, M. R. Zanotelli, S. Somasegar, J. P. Califano, C. Montague, D. J. LaValley, J. Huynh, N. Mencia-Trinchant, Y. L. Negrón Abril, D. C. Hassane, L. J. Bonassar, J. T. Butcher, R. S. Weiss and C. A. Reinhart-King, *Proc. Natl. Acad. Sci.*, 2017, **114**, 492–497.

15 J. M. Fleming, S. T. Yeyeodu, A. McLaughlin, D. Schuman and D. K. Taylor, *ACS Chem. Biol.*, 2018, **13**, 2825–2840.

16 A. G. Waks and E. P. Winer, *JAMA*, 2019, **321**, 288–300.

17 C. Gialeli, A. D. Theocharis and N. K. Karamanos, *FEBS J.*, 2011, **278**, 16–27.

18 M. Nilsson, H. Adamo, A. Bergh and S. Halin Bergström, *Sci. Rep.*, 2016, **6**, 19608.

19 J. Riegler, Y. Labyed, S. Rosenzweig, V. Javinal, A. Castiglioni, C. X. Dominguez, J. E. Long, Q. Li, W. Sandoval, M. R. Junttila, S. J. Turley, J. Schartner and R. A. D. Carano, *Clin. Cancer Res.*, 2018, **24**, 4455–4467.

20 A. Pan, Z. Wang, B. Chen, W. Dai, H. Zhang, B. He, X. Wang, Y. Wang and Q. Zhang, *Drug Deliv.*, 2018, **25**, 1495–1503.

21 S. Pal, *Design of Artificial Human Joints & Organs*, Springer US, Boston, MA, 2014.

22 L. Qian and H. Zhao, *Micromachines*, 2018, **9**, 654.

23 E. A. Klein, L. Yin, D. Kothapalli, P. Castagnino, F. J. Byfield, T. Xu, I. Levental, E. Hawthorne, P. A. Janmey and R. K. Assoian, *Curr. Biol.*, 2009, **19**, 1511–1518.

24 J. Weickenmeier, R. de Rooij, S. Budday, P. Steinmann, T. C. Ovaert and E. Kuhl, *Acta Biomater.*, 2016, **42**, 265–272.

25 A. Tang, G. Cloutier, N. M. Szeverenyi and C. B. Sirlin, *AJR Am. J. Roentgenol.*, 2015, **205**, 22–32.

26 L. E. Bilston, *NMR Biomed.*, 2018, **31**, e3832.

27 J. Solon, I. Levental, K. Sengupta, P. C. Georges and P. A. Janmey, *Biophys. J.*, 2007, **93**, 4453–4461.

28 D. Chester, R. Kathard, J. Nortey, K. Nellenbach and A. C. Brown, *Biomaterials*, 2018, **185**, 371–382.

29 K. Tan, S. Cheng, L. Jugé and L. E. Bilston, *J. Biomech.*, 2013, **46**, 1060–1066.

30 J. P. Winer, S. Oake and P. A. Janmey, *PLoS ONE*, 2009, **4**, e6382.

31 M. S. Hall, F. Alisafaei, E. Ban, X. Feng, C.-Y. Hui, V. B. Shenoy and M. Wu, *Proc. Natl. Acad. Sci. U. S. A.*, 2016, **113**, 14043–14048.

32 L. J. Kaufman, C. P. Brangwynne, K. E. Kasza, E. Filippidi, V. D. Gordon, T. S. Deisboeck and D. A. Weitz, *Biophys. J.*, 2005, **89**, 635–650.

33 A. Pathak and S. Kumar, *Integr. Biol.*, 2011, **3**, 267.

34 K. L. Mills, R. Kemkemer, S. Rudraraju and K. Garikipati, *PLoS One*, 2014, **9**, e103245.

35 S. R. Polio, A. N. Kundu, C. E. Dougan, N. P. Birch, D. E. Aurian-Blajeni, J. D. Schiffman, A. J. Crosby and S. R. Peyton, *PLOS ONE*, 2018, **13**, e0204765.

36 F. L. Jayes, B. Liu, F. T. Moutos, M. Kuchibhatla, F. Guilak and P. C. Leppert, *Am. J. Obstet. Gynecol.*, 2016, **215**, 596.e1-596.e8.

37 R. D. Corder, S. V. Gadi, R. B. Vachieri, F. L. Jayes, J. M. Cullen, S. A. Khan and D. K. Taylor, *Acta Biomater.*, 2021, **134**, 443–452.

38 C. D. Madsen and T. R. Cox, *Bio-Protoc.*, 2017, **7**, e2265.

39 E. Lamers, T. H. S. van Kempen, F. P. T. Baaijens, G. W. M. Peters and C. W. J. Oomens, *J. Mech. Behav. Biomed. Mater.*, 2013, **28**, 462–470.

40 R. W. Chan, *J. Rheol.*, 2018, **62**, 695–712.

41 E. Linetsky, R. Bottino, R. Lehmann, R. Alejandro, L. Inverardi and C. Ricordi, *Diabetes*, 1997, **46**, 1120–1123.

42 F. Bertuzzi, S. Cainarca, S. Marzorati, A. Bachi, B. Antonioli, R. Nano, R. Verzaro and C. Ricordi, *Cell Transplant.*, 2009, **18**, 203–206.

43 A. Dua and S. S. Desai, *J. Histol.*, 2013, **2013**, 1–5.

44 D. K. Taylor, F. L. Jayes, A. J. House and M. A. Ochieng, *J. Funct. Biomater.*, 2011, **2**, 173–194.

45 Z. Ma, D. M. Nelson, Y. Hong and W. R. Wagner, *Biomacromolecules*, 2010, **11**, 1873–1881.

46 C. Tonhauser, C. Schüll, C. Dingels and H. Frey, *ACS Macro Lett.*, 2012, **1**, 1094–1097.

47 M. Sztalmachova, J. Gumulec, M. Raudenska, H. Polanska, M. Holubova, J. Balvan, K. Hudcova, L. Knopfova, R. Kizek, V. Adam, P. Babula and M. Masarik, *Int. J. Oncol.*, 2015, **46**, 1810–1818.

48 B. L. Carlson, J. L. Pokorny, M. A. Schroeder and J. N. Sarkaria, *Curr. Protoc. Pharmacol.*, 2011, **52**, 1–14.

49 D. E. Pegg, *Cryobiology*, 2020, **93**, 3–11.

50 R. H. Ewoldt, A. E. Hosoi and G. H. McKinley, *J. Rheol.*, 2008, **52**, 1427–1458.

51 M. Rubinstein and R. H. Colby, *Polymer Physics*, Oxford University Press, New York, 2003.

52 A. Nabavizadeh, M. Bayat, V. Kumar, A. Gregory, J. Webb, A. Alizad and M. Fatemi, *Sci. Rep.*, 2019, **9**, 5737.

53 H. Dehghani, R. Penta and J. Merodio, *Mater. Res. Express*, 2018, **6**, 035404.

54 M. Deville, R. Natalini and C. Poignard, *Bull. Math. Biol.*, 2018, **80**, 3184–3226.

55 J. J. Arroyo-Crespo, A. Armiñán, D. Charbonnier, C. Deladriere, M. Palomino-Schätzlein, R. Lamas-Domingo, J. Forteza, A. Pineda-Lucena and M. J. Vicent, *Int. J. Cancer*, 2019, **145**, 2267–2281.

56 K. S. Cho, K. Hyun, K. H. Ahn and S. J. Lee, *J. Rheol.*, 2005, **49**, 747–758.

57 H. T. Lim, K. H. Ahn, J. S. Hong and K. Hyun, *J. Rheol.*, 2013, **57**, 767–789.